SMC-TR-94-06

AEROSPACE REPORT NO.
TR-93(3935)-2

Soft X-Ray Photoelectron Spectroscopy Study of the Interaction of Cr with $MoS_2(0001)$

14 January 1994

Prepared by

T. D. DURBIN, J. R. LINCE, and S. V. DIDZIULIS
Mechanics and Materials Technology Center
Technology Operations

D. K. SHUH and J. A. YARMOFF
Materials Sciences Division
Lawrence Berkeley Laboratory
Berkeley

Prepared for

SPACE AND MISSILE SYSTEMS CENTER
AIR FORCE MATERIEL COMMAND
2430 E. El Segundo Boulevard
Los Angeles Air Force Base, CA 90245

Engineering and Technology Group

This report was submitted by The Aerospace Corporation, El Segundo, CA 90245-4691, under Contract No. F04701-88-C-0089 with the Space and Missile Systems Center, 2430 E. El Segundo Blvd., Los Angeles Air Force Base, CA 90245. It was reviewed and approved for The Aerospace Corporation by S. Feuerstein, Principal Director, Mechanics and Materials Technology Center. Capt. Mark Borden, SMC/CIE, was the project officer for the Mission-Oriented Investigation and Experimentation (MOIE) program.

This report has been reviewed by the Public Affairs Office (PAS) and is releasable to the National Technical Information Service (NTIS). At NTIS, it will be available to the general public, including foreign nationals.

This technical report has been reviewed and is approved for publication. Publication of this report does not constitute Air Force approval of the report's findings or conclusions. It is published only for the exchange and stimulation of ideas.

JOHN A. GOYETTE, Col, USAF
System Program Director
Defense Meteorological Satellite Program

Wm. Kyle Sneddon, Captain USAF
Deputy, Industrial & International Division

REPORT DOCUMENTATION PAGE

Form Approved
OMB No. 0704-0188

1. AGENCY USE ONLY (*Leave blank*)	2. REPORT DATE	3. REPORT TYPE AND DATES COVERED
	14 January 1994	

4. TITLE AND SUBTITLE
Soft X-ray Photoelectron Spectroscopy Study of the Interaction of Cr with MoS_2(0001)

5. FUNDING NUMBERS
F04701-88-C-0089

6. AUTHOR(S)
Durbin, Thomas D.; Lince, Jeffrey R.; Didziulis, Stephen V.; Shuh, David K.; Yarmoff, Jory A.

7. PERFORMING ORGANIZATION NAME(S) AND ADDRESS(ES)
The Aerospace Corporation
Technology Operations
El Segundo, CA 90245-4691

8. PERFORMING ORGANIZATION REPORT NUMBER
TR-93(3935)-2

9. SPONSORING/MONITORING AGENCY NAME(S) AND ADDRESS(ES)
Space and Missile Systems Center
Los Angeles Air Force Base
Los Angeles, CA 90009-2960

10. SPONSORING/MONITORING AGENCY REPORT NUMBER
SMC-TR-94-06

11. SUPPLEMENTARY NOTES

12a. DISTRIBUTION/AVAILABILITY STATEMENT
Approved for public release; distribution unlimited

12b. DISTRIBUTION CODE

13. ABSTRACT (*Maximum 200 words*)

The solid lubricant MoS_2 must exhibit good adhesion to high-Cr steels used in moving mechanical assemblies on spacecraft to provide an effective antiwear lifetime. The adhesion can be maximized by tailoring the interfacial reactivity between the Cr at the steel surface and MoS_2. To this end, we studied the interaction of Cr with the MoS_2(0001) surface with core-level and valence-band soft X-ray photoelectron spectroscopy employing synchrotron radiation (hν=150 to 400 eV). Cr vapor-deposited at room temperature formed relatively flat films on MoS_2(0001). The Cr underwent a limited chemical reaction with the MoS_2 substrate to form a chromium sulfide and Mo metal. The Mo metal formed a thin layer between the Cr film and the MoS_2 substrate. In contrast, reacted S was incorporated throughout the Cr film, with its concentration enhanced at the surface. Annealing the Cr-covered sample drove the reaction between Cr and MoS_2, forming additional Mo metal that alloyed with Cr, and several adsorbed S species on the Cr film surface. Annealing also caused partial coalescence of the Cr-containing portion of the film, uncovering parts of the Cr-Mo alloy. The reactivity of Cr with respect to MoS_2(0001) is greater than that of Fe and somewhat less than that of Mn. The results indicate that cleaning the surface of a steel device before MoS_2 film deposition will expose bare Fe and Cr metal, which could increase the metal/lubricant adhesion.

14. SUBJECT TERMS
Molybdenum disulfide, Chromium, Photoelectron spectroscopy, Solid lubricants, Interfacial chemistry, Synchrotron radiation

15. NUMBER OF PAGES
38

16. PRICE CODE

17. SECURITY CLASSIFICATION OF REPORT	18. SECURITY CLASSIFICATION OF THIS PAGE	19. SECURITY CLASSIFICATION OF ABSTRACT	20. LIMITATION OF ABSTRACT
UNCLASSIFIED	UNCLASSIFIED	UNCLASSIFIED	

PREFACE

This work was supported by the Air Force Materiel Command, Space and Missile Systems Center under contract No. F04-701-88-C-0089. The SXPS experiment was conducted at the National Synchrotron Light Source, Brookhaven National Laboratory, which is supported by the U.S. Department of Energy (Division of Materials Sciences and Division of Chemical Sciences, Basic Energy Sciences) under Contract No. DE-AC02-76CH00016.

CONTENTS

FIGURES

TABLES

1. INTRODUCTION

Many moving mechanical assemblies on satellites increasingly use a solid lubricant formulation based on sputter-deposited films of molybdenum disulfide (MoS_2). Presently, these films are used on actuators and deployment mechanisms, and other uses are planned. The effectiveness of sputter-deposited MoS_2 as well as other MoS_2 formulations such as burnished or spray-bonded films is dependent on the ability of the lubricant to adhere strongly to the substrate, such as the surface of a bearing or latch.

Strong adhesion between a film and its substrate is related to the chemical bonding and reactivity between the two. By finding ways to control this reactivity, through appropriate surface treatments, the adhesion and therefore the effectiveness of the lubricated device can be optimized. MoS_2 is often used on devices made of steels consisting of Fe and Cr. We investigated the chemical interaction of Fe with MoS_2 in previous studies; in the present study, we report on continuing investigations of the Cr/MoS_2 interface.

In general, the interaction of transition metals with the MoS_2(0001) basal-plane surface has been the subject of extensive study because of the utility of MoS_2 in catalysis and electronic materials as well as tribology.[1-9] MoS_2 is a semiconducting, transition-metal dichalcogenide compound that crystallizes in S-Mo-S "sandwich" layers. Within the layers, there is strong covalent bonding, but the layers are bound to one another by weaker van der Waals forces. This structure makes MoS_2 an excellent solid lubricant since the layers form effective slip planes. Cleavage between these layers reveals the highly inert MoS_2(0001) basal-plane surface, which is S-terminated.

Previous studies have shown that MoS_2(0001) is more inert with respect to chemical reaction with deposited metals than other semiconductors. Strong (i.e., bulk) reaction of metals with MoS_2 may be described by the following reaction:

$$metal + \left(\frac{b}{2a}\right)MoS_2 \rightarrow \left(\frac{1}{a}\right)metal_aS_b + \left(\frac{b}{2a}\right)Mo \qquad (1)$$

Based on bulk thermodynamics, the reactions of Al and V with MoS_2 are favorable at 25 °C (i.e., have negative $\Delta G_{reaction}$'s), but neither reacts strongly with the MoS_2(0001) surface.[1,5] Other metals with negative or small positive $\Delta G_{reaction}$'s at 25 °C, such as Cu,[5] In,[1,5] Pd,[1,8] Fe,[1,2,6,7] and Ni,[4,5] are either nonreactive or only minimally reactive with MoS_2(0001). The only metals that have shown strong reactivity are Mg,[5] Ti,[5] and Mn.[1,3] Clearly, thermodynamic considerations alone are not a sufficient indicator of reactivity at the metal/MoS_2(0001) interface, and further study is needed to learn how kinetics and/or surface energy factors are involved.

The formation of Cr films up to 100 Å thick on MoS_2(0001) in ultra-high vacuum (UHV) was studied previously.[9] X-ray photoelectron spectroscopy (XPS) was used to determine the

chemical composition of the film, and scanning auger microscopy (SAM) was used to investigate the morphology as well as the lateral and depth distributions of Cr, S, and Mo. The capability of XPS in identifying reaction products on the surface is limited, however, by the resolution and larger sampling depth of XPS compared to soft X-ray photoelectron spectroscopy (SXPS).

In the study presented here, the interaction of Cr metal with $MoS_2(0001)$ in UHV was studied with SXPS employing synchrotron radiation and low-energy electron diffraction (LEED). Film thicknesses up to 17 Å were studied. Core-level spectra were taken with varying photon energies to probe different depths of the surface region, obtaining a qualitative depth profile. Valence-band spectra were used as a sensitive probe of both the chemical state and the degree of metallic character in the surface region.

The results of the present work agree with those of Ref. 9. The present results suggest that vapor-deposited Cr forms relatively flat films, undergoing a limited chemical interaction between Cr and MoS_2. This interaction results in the formation of a chromium sulfide compound and metallic Mo. Chromium sulfide is incorporated into the Cr overlayer, with strong enhancement of S at the surface. In contrast, metallic Mo is found only at the interface. Annealing a Cr-covered sample further drives the reaction between Cr and MoS_2. The results of these two studies can be combined to better understand the chemistry at the metal/$MoS_2(0001)$ interface and to learn ways to enhance the adhesion of MoS_2-based solid lubricants to high-Cr steel surfaces.

2. EXPERIMENTAL

$MoS_2(0001)$ basal-plane surfaces were prepared by cleavage of natural molybdenite crystals (obtained from Wards Natural Science Establishment) in air. The samples were mounted between two Ta clips for resistive heating and were cleaned by annealing to 700 °C for 10 minutes. The temperature was measured with an infrared pyrometer through a sapphire window. This annealing procedure has been shown to produce clean, defect-free surfaces.[2,3,10] SXPS spectra collected from these surfaces showed sharp S 2p and Mo 3d core levels, indicative of clean, unreacted $MoS_2(0001)$, and there was no evidence of impurities.

Cr (99.99% purity) was evaporated onto the sample from a tungsten wire basket in a sample preparation chamber that has a base pressure of $5x10^{-10}$ torr. The pressure was typically in the mid-10^{-9} torr range during deposition with the sample at room temperature. After each deposition, the sample was transferred under UHV into the spectrometer chamber (base pressure = $1x10^{-10}$ torr) where the SXPS spectra were collected.

The data were collected on beamline UV-8b at the National Synchrotron Light Source, Brookhaven National Laboratory, with an ellipsoidal mirror analyzer operating in an angle-integrating mode.[11] Monochromatic photons were generated with a 10-m toroidal grating monochromator.[12] The spectra were normalized to the incident photon flux by dividing by the photoelectron current measured from the (C-contaminated) Au-coated final focusing mirror. Although this normalization technique is adequate to correct for fluctuations in the beam current, it does not account for variations in repositioning the sample that occur when the sample is removed from the spectrometer for incremental Cr deposition. Therefore, changes in the absolute intensities were used only to determine the approximate film thicknesses. To determine the changes in the relative amounts of the various chemical species within the SXPS detection volume, ratios between peaks in spectra collected without moving the sample were used.

Photon energies for the Mo 3d and S 2p core-level spectra were chosen to produce two different photoelectron kinetic energies. The Mo 3d spectra were collected with photon energies of both 300 and 400 eV, producing photoelectrons with kinetic energies of ~70 and ~170 eV, respectively. The S 2p spectra were taken with photon energies of 230 and 330 eV, also giving photoelectron kinetic energies of ~70 and ~170 eV. As a result, the same depths were probed for the Mo 3d and S 2p spectra. The approximate escape depths for different photoelectron kinetic energies were calculated using a formula developed by Tanuma and coworkers.[13] The values are 3.0 Å for the Mo 3d and S 2p spectra collected at ~70 eV photoelectron kinetic energy, 3.5 Å for the Cr 3p and Mo 4p spectra collected at ~100 eV, and 4.7 Å for the Mo 3d and S 2p collected at ~170 eV. Since the analyzer is operated in an angle-integrating mode, these escape depths are averaged over the 86° emission cone (a solid angle of $\sim\pi/2$ steradians) centered about the sample normal.

The Mo 3d and S 2p spectra were analyzed with a least-squares curve fitting procedure to determine the binding energies, widths, and relative peak areas of the various core-level components. Before deconvoluting the core-level spectra, a background representing the

secondary electron yield was subtracted from the raw data.[14] The resultant spectrum was then fit to a sum of Gaussian-broadened Lorentzian line shapes.

Before fitting the entire set of Mo 3d and S 2p core levels, Mo 3d and S 2p core levels collected from the clean surface were fit to determine the branching ratio and spin-orbit energy splitting for respective spin-orbit components, as well as the Lorentzian widths for all the components. The Mo 3d and S 2p spectra collected with photon energies of 300 and 230 eV, respectively, (i.e., the ~70 eV kinetic energy spectra) were used to determine these values, since they were better resolved than the corresponding spectra collected at higher photon energies. The peak separation and branching ratio between the Mo $3d_{5/2}$ and $3d_{3/2}$ spin-orbit components were 3.14 eV and 1.43, respectively. The corresponding parameters for the S $2p_{3/2}$ and $2p_{1/2}$ spin-orbit components were 1.19 eV and 2.00. These parameters are similar to those used previously for deconvolution of Mo 3d and S 2p core levels.[2,3,15] The Lorentzian widths were determined to be 0.06 eV for the Mo $3d_{5/2}$ component, 0.28 eV for the Mo $3d_{3/2}$ component, 0.05 eV for the S $2p_{3/2}$ component and 0.06 eV for the S $2p_{1/2}$ component. In fitting the spectra from the Cr-covered surfaces, the spin-orbit parameters and Lorentzian components of the widths were constrained at the values determined from the clean surface. The Gaussian components of the widths, along with the peak areas and positions, were determined separately for each spectrum.

The Cr 3p core level spectra were also analyzed using curve fitting. These levels were only analyzed to determine the relative area under the peaks, however, and not to determine the individual chemical components that make up the peak shape. Since the spin-orbit separation is small for the Cr 3p level,[16] a single peak was used for these fits. It should be noted that these peaks were asymmetric due to their metallic nature (i.e., the Doniach-Sunjic lineshape[17]).

The Cr film thicknesses were calibrated by using the attenuation of the Mo 3d substrate signal via the following relation:[18]

$$I = I_0 e^{\left(-\frac{t}{l}\right)} \tag{2}$$

where I is the photoelectron peak area of the Mo 3d substrate component collected after each deposition, I_0 is the photoelectron peak area of the Mo 3d substrate component collected from the clean surface, l is the photoelectron escape depth, and t is the film thickness. Since this equation is only applicable for uniform films, the reported thicknesses are only accurate to about ±25%. There is also some error associated with the difficulty in reproducing the sample position after each deposition, as discussed above. This error is expected to be small, however, compared to the error resulting from film nonuniformity. The film thicknesses were determined using Mo 3d substrate components collected with a ~170 eV photoelectron kinetic energy since spectra collected with ~70 eV electrons are more sensitive to non-uniformities in the film thickness.

3. RESULTS

3.1 CORE-LEVEL SPECTROSCOPY

3.1.1 Deposition of Cr Films on $MoS_2(0001)$

Figure 1 shows representative SXPS spectra, along with numerical fits, of the Mo 3d core level after Cr deposition. Spectra were collected with photon energies of both 300 and 400 eV, producing photoelectrons with kinetic energies of ~70 and ~170 eV, respectively. Since the results of the high and low kinetic energy spectra are qualitatively similar, only the 70 eV spectra are shown. A summary of the binding energies obtained from the numerical fits of all of the 70 eV spectra collected after various stages of Cr deposition is shown in Table 1.

After deposition of 2 Å of Cr, the substrate Mo 3d component shifts 0.4 eV toward lower binding energy because of band bending, and a second Mo 3d component appears at a binding energy that is ~0.9 eV lower than the shifted substrate component. This second Mo species is identified as Mo metal since its binding energy is similar to that observed previously for metallic Mo on MoS_2.[3,19] The metallic Mo peak is seen in Fig. 1(b), which was acquired after deposition of 5 Å of Cr. The appearance of this second peak indicates that Cr is reacting with $MoS_2(0001)$ and decomposing the substrate to produce elemental Mo.

Cr 3p and Mo 4p core-level spectra are shown in Fig. 2. As the thickness of the film increases, the Cr 3p peak area increases relative to the Mo 4p area. In the spectra collected from 5 and 9 Å films, the Mo 4p signal is barely detectable above the noise level. After a 17 Å Cr film has been deposited, the Mo 4p core level is virtually undetectable. The disappearance of the detected Mo is shown more clearly by the Mo/Cr ratio, which is plotted in Fig. 3(a). (The Mo 3d core level was used to calculate the Mo/Cr ratio because its photoelectron cross section is greater than that for the Mo 4p; cross sections were obtained from Ref. 20.) The quantity of Mo present in the SXPS detection volume after deposition of a 17 Å Cr film is shown to be 0.2% of that for detected Cr. This indicates that both the substrate and metallic Mo are covered by a Cr overlayer whose thickness is larger than several photoelectron escape depths. Therefore, the metallic Mo is present primarily near the film/substrate interface. In contrast, the S 2s peak area increases greatly compared with that for Mo 3d (Fig. 1), showing that sulfidic products of the Cr/MoS_2 reaction are incorporated in the Cr overlayer and/or on its surface. The asymmetry of the Cr 3p spectrum is due partly to the presence of these sulfides and partly to the metallic nature of the remaining unreacted Cr (see Section 2).

The evolution of the metallic Mo peak area divided by the substrate Mo peak area is shown in Fig. 4 for both 70 and 170 eV photoelectrons. The figure shows graphically that the relative amount of metallic Mo increases fairly monotonically with increasing coverage. Comparison of the ratios between low and high photoelectron kinetic energy can help determine the morphology of the metallic Mo (which was shown above to exist near the film/substrate interface). In Fig. 4, the two ratios follow each other within experimental error. Preliminary calculations were conducted to model the Mo(metal)/Mo(substrate) ratio versus coverage, assuming a uniform Mo(metal) film forms on top of the substrate. This model gives a ratio for 70 eV photoelectron kinetic energy that is significantly greater than that for 170 eV kinetic energy. Therefore, Fig. 4

shows that metallic Mo does not form a uniform film on top of the substrate. Rather, it forms islands on the substrate beneath the Cr film. Whether the islands are interconnected (i.e., to form a complete, but nonuniform film) cannot be accurately determined using this analysis.

Evidence of Cr chemical interaction with the substrate is also clearly visible in the S 2p core-level spectra, shown in Fig. 5. The broadening of the raw S 2p data and filling in of the gap between the deconvoluted S $2p_{3/2}$ and $2p_{1/2}$ components during Cr deposition indicate the formation of a second S species. Also, the S 2p spectra of samples with lower Cr coverages could not be fit adequately with a single chemical species. Instead, two doublets, ~0.1 eV apart in binding energy, were used to fit the data. The necessity of including a second S peak is readily apparent since the S 2p spectrum remains relatively intense even after the substrate is covered. In addition, fitting showed that the substrate peak monotonically fell to essentially zero intensity—its inclusion in the fits was not necessary for the highest coverages. Therefore, the lower binding energy S 2p component most likely has contributions from one or more chromium sulfide compounds. Note that for all thicknesses, the positions of the two peaks were fixed (Table 1). (The fixed values were determined by preliminary fitting of the entire set of S 2p core levels.) This ensured that peak area variations between successive spectra were not the result of variations in the peak positions during the fitting procedure. The Gaussian widths of each of the two components remained essentially constant throughout the fitting procedure, i.e., they varied by $\leq$0.2 eV.

The formation of a Cr sulfide is supported by Fig. 3(b), which shows that S represents a non-negligible fraction (~40%) of the Cr film in the region of the SXPS detection volume. This is in contrast to Mo, which only represents a minuscule fraction (0.2%) of the surface of the 17 Å Cr film [Fig. 3(a)]. This confirms that no substrate peak is present in the S 2p spectrum at high Cr coverages.

After growing a 5 Å film, a small S 2p component appeared at a binding energy 1.4 eV higher than that of the substrate component [see Table 1 and Figs. 5 (c) and (d)]. This peak may indicate the formation of a polysulfide species [denoted here as $(S\text{-}S)^{2-}$]. Such a species could form if two or more S atoms bond to each other to form an ion with a 2- charge, resulting in an oxidation state per atom that is lower than that for the S^{2-} ion. In fact, the large width of this peak suggests that more than one polysulfide species is present, each with a different number of S atoms. The difference between the $(S\text{-}S)^{2-}$ (specifically, a polysulfide ion with two S atoms) and S^{2-} binding energies was previously reported to be 1.1 eV in amorphous MoS_3, approximately the difference observed here.[21] A similar feature, also assigned to $(S\text{-}S)^{2-}$ formation, was seen in other studies of $MoS_2(0001)$ surfaces.[2,15]

The chromium sulfide(s) produced during a Cr/MoS_2 reaction could be any of a number listed in the literature, including CrS, Cr_2S_3, Cr_3S_4, Cr_5S_6, and Cr_7S_8.[22-24] The use of equation (1) shows that both CrS and Cr_3S_4 are products of thermodynamically favorable reactions of Cr with MoS_2 ($\Delta G_{reaction}$ = -10±4 and -9±5 kcal/mol, respectively). The formation of Cr_2S_3 is also possible since its reaction is only slightly unfavorable ($\Delta G_{reaction}$ = 8±8 kcal/mole).[25,26] Note that it is possible that some of the metallic Mo might dissolve in the Cr and the resultant heat of solution could make the reaction slightly more favorable. However, the extent of dissolution is not known for such thin films, so the effect on $\Delta G_{reaction}$ is difficult to quantify.

Although it is difficult to identify a single chromium sulfide species from these bulk thermodynamic results, some idea of the species present can be obtained from the binding energy data in the present study. There have been no single studies in the literature that compare MoS_2 and CrS binding energies, but these differences can be estimated by cross-referencing separate studies that compare the S 2p binding energies of MoS_2 and CrS to a common compound. It was determined that the binding energy of the S 2p core level of MoS_2 is 0.5 eV higher than that of MnS.[3] In a separate study, it was determined that the S 2p binding energy for CrS is 0.7 eV higher than that of MnS.[27] The S 2p binding energy in CrS should, therefore, be ~0.2 eV higher than that of MoS_2. The S 2p component we identified as a Cr-S compound in the present study is ~0.1 eV lower in binding energy than S 2p in MoS_2, so this represents a difference between the measured binding energy and the estimate of ~0.3 eV. This difference could be due to surface versus bulk effects, or the chromium sulfide present might differ slightly from a 1:1 stoichiometry (e.g., Cr_7S_8). In addition, a range of stoichiometries may exist. Note that the only other compound with available binding energy data is Cr_2S_3, and its S 2p binding energy was measured to be 1.1 eV lower in binding energy than that of MoS_2.[28] The presence of oxygen in the form of sulfates on the Cr_2S_3 surface may have affected those results, however.

Comparison of photoelectron data taken at different photon energies, and therefore different photoelectron kinetic energies, can indicate qualitative differences in the distribution of chemical species with depth beneath the sample surface. Fig. 6(b) shows the ratio of the total Mo 3d peak area for low photoelectron kinetic energy (70 eV) to that for high photoelectron kinetic energy (170 eV). Fig. 6(a) shows the corresponding ratio for the low and high kinetic energy (also 70 and 170 eV) S 2p peaks. The curves were normalized so that at zero coverage the ratios were equal to 1.0 for both S and Mo. This was done so that qualitative changes in surface enhancement (or depletion) of S and Mo during Cr deposition could be related to a standard surface, that of the clean $MoS_2(0001)$ surface. The densities of both S and Mo are constant perpendicular to the surface in MoS_2, so the actual ratios should be close to 1.0 for the clean $MoS_2(0001)$ surface. During the Cr deposition and resultant annealing, values >1.0 (or <1.0) represent S or Mo that is enhanced (or depleted) at the surface.

The curve for Mo [Fig. 6(b)] shows that increasing Cr coverage gives rise to an Mo depth distribution that is increasingly enhanced below the surface compared to pure $MoS_2(0001)$. This agrees with our conclusion earlier in this section that the reacted Mo is present below the Cr film on the unreacted portion of the substrate. Therefore, as the Cr film grows thicker, the location of the metallic Mo is increasingly far from the surface of the Cr film.

In contrast, the curve for S [Fig. 6(a)] reveals that S is significantly enhanced at the surface of the Cr film for all Cr coverages. This surface enhancement is caused by diffusion of S to the Cr film surface after chemical reaction between the Cr and MoS_2 substrate. This agrees with the conclusion reached earlier in this section, as well as with the results from an earlier SAM sputter-depth-profile study of thicker Cr films on $MoS_2(0001)$ that revealed that the S concentration was enhanced at the surface of the Cr film.[9] The diffusion of S to the surface of metals is common and has been seen for Cr, Ni, Cu, and Fe.[29,30]

Based on the results of this section and the results of Ref. 9, a schematic diagram of the formation of the Cr overlayer during deposition is shown in Fig. 7(b). Note that Fig. 7 is based on results of both the XPS/SAM study[9] and the present study.

3.1.2 Annealing the 17 Å Cr film on $MoS_2(0001)$

The evolution of the Mo 3d core level on annealing a 17 Å Cr film is shown in Fig. 8. Annealing to 425 °C caused the area of the Mo(metal) component to increase considerably compared with that of the S 2s [Fig. 8(b)] and the Cr 3p [Fig. 3(a)]. The increase in the metallic Mo signal is caused partly by an increase in the amount of metallic Mo present at the film-substrate interface. In addition, the Cr film may agglomerate slightly such that the metallic Mo at the interface is more easily detected. However, the amount of agglomeration is small since the Mo detected is still <6% of the detected Cr [Fig. 3]. These results agree with those in a previous study of Cr on $MoS_2(0001)$, which showed that little agglomeration of the Cr overlayer occurs on annealing to low temperatures.[9]

There is an asymmetry to the Mo(metal) spectrum (i.e., higher intensity on the high binding energy side) due to electronic losses, which are greater for metallic species. We have simulated this Doniach-Sunjic lineshape[17] by including a broad peak on the high binding energy sides of the main peak. Note that the position of this peak does not correspond well to that of the Mo 3d for MoS_2. However, a small MoS_2 substrate contribution might be present in the left side of this loss region (the presence of a small amount of substrate is shown by LEED results discussed below).

There is a large drop in the detected S/Mo ratio on annealing to 425 °C, as seen in Figs. 8(a) and 8(b). Note that the change in these spectra is due to a large increase in *detected* Mo. In fact, the amount of S actually increases, as shown by the increase in the S/Cr ratio in Fig. 3(b).

The S 2p core-level spectra collected after annealing are shown in Fig. 9. After annealing to 425 °C, the S 2p core level has two major components [Fig. 9(b)]. The largest component probably represents the reacted Cr-S species present before the anneal. This peak is shifted only slightly from its position before the anneal (see Table 2). The second component appears 0.8 eV lower in binding energy than the largest component. The peak area of this second species is enhanced by 30% in the low kinetic energy S 2p spectrum relative to that in the less surface sensitive, high kinetic energy spectrum, as shown in Fig. 10. This difference shows that the concentration of this second species is enhanced at the surface. This second species is most likely S adsorbed on the surface of the Cr overlayer [denoted S(adsorbed,1) in Fig. 9(b)]. It is unlikely that it is related to Mo, since there is little Mo on which S can adsorb after this anneal [Fig. 3].

Additional changes in the core-level spectra occur on annealing to higher temperatures. After annealing to 700 °C, and subsequently to 850 °C, there is a large increase in the Mo/Cr ratio [Fig. 3(a)]. The increase is caused by a large increase in the amount of S incorporated into the Cr film [Fig. 3(b)], as well as an increase in the formation of metallic Mo [probably forming a Cr-Mo alloy, as discussed below and shown schematically in Fig. 7(d)]. This result for higher-temperature anneals agrees with the results of the XPS/SAM study.[9] In that study, it was shown that annealing the sample to higher temperatures (i.e., >650 °C) drove the reaction between Cr and MoS_2 and caused the Cr-containing portion of the reacted film to coalesce appreciably.

The Mo 3d spectra taken after annealing to 700 °C and then to 850 °C [Figs. 8(c) and (d), respectively] exhibit a shift 0.4-0.5 eV lower in binding energy compared to that taken for the 425 °C anneal [Fig. 8(b) and Table 2]. This shift is most likely due to the formation of a Cr-Mo alloy. The presence of an alloy is supported by the fact that Cr and Mo form a continuous solid

solution.[31] The metallicity of this species is confirmed by the asymmetric Doniach-Sunjic lineshape in the Mo 3d spectra. A small, broad peak is included on the high binding energy side of the main peak to compensate for this asymmetry, similar to the spectrum for the 425 °C anneal shown in Fig. 8(b).

Annealing to 700 °C and 850 °C also induced changes in the S 2p level, now composed of three major species [Figs. 9(c) and (d)]. The Cr-S component remains the largest component. The second and third components in the spectra are 0.6 and 1.3 eV lower in binding energy, respectively, than the Cr-S peak. Both of these two additional species are enhanced in the low kinetic energy spectrum compared to the high kinetic energy spectrum (see Fig. 11) relative to the highest binding energy peak representing the Cr-S peak. This relative enhancement demonstrates that the two lower binding energy species represent adsorbed S phases [denoted S(adsorbed,2) and S(adsorbed,3) in Figs. 9(c) and (d)]. These species probably represent different binding sites or states than the adsorbed S seen for the 425 °C anneal, since the binding energies of both S(adsorbed,2) and S(adsorbed,3) are different from that of S(adsorbed,1). Note that it is likely that neither S(adsorbed,2) nor S(adsorbed,3) represents S adsorbed on the parts of the Cr-Mo alloy film that were uncovered by the anneal, since no corresponding additional Mo species were seen in the Mo 3d spectrum other than the pure Cr-Mo alloy contribution.

The evolution of the Cr 3p and Mo 4p core levels on annealing the Cr-covered surface is shown in Fig. 2. Annealing to 425 °C resulted in the reappearance of the Mo 4p level at a binding energy 2.0 eV lower than that of the clean substrate Mo 4p, indicating metallic Mo formation, which is consistent with the behavior of the Mo 3d core level. Annealing the surface to 700 °C and then to 850 °C resulted in an increase in intensity on the high binding energy side of the metallic Cr 3p peak. This confirms that annealing the sample induced the formation of increasing amounts of reacted Cr-S species in the film. The large width of this shoulder is due to the presence of several reacted Cr-S species [i.e., the three states seen in Figs. 9(c) and (d)]. The shape of the Cr 3p spectrum suggests that a small amount of metallic Cr may still exist. This metallic Cr may be entirely contained within the Cr-Mo alloy.

3.2 LOW-ENERGY ELECTRON DIFFRACTION

The deposition of a Cr film caused the substrate 1 × 1-(0001) LEED pattern to disappear, showing that the Cr overlayer is polycrystalline or amorphous. Annealing the sample to 425 °C resulted in the reappearance of the pattern, indicating that portions of the substrate are either uncovered or only covered by thin regions of the agglomerating film. The spots are diffuse, however, and there is a high background intensity, suggesting that only small domains of the substrate are uncovered. After annealing to 700 °C, the pattern and spot size were similar to the previous LEED pattern, but with somewhat more intense spots. This indicates that there are more patches of uncovered substrate, but no large increase in the average domain size. Annealing the sample to 850 °C resulted in a more intense LEED pattern with a spot size approximately one-half the spot size observed previously. This suggests that the substrate patches are greater in number and have an average domain size approximately twice that present after the previous anneal.

The presence of MoS_2(0001) substrate seen with LEED after annealing does not contradict the SXPS results that show that the MoS_2 substrate-related feature is virtually undetectable after

annealing (see Fig. 8). LEED is sensitive to very small amounts of order, i.e., to a few percent of the total surface area in the surface region, while a similar proportion of the substrate is not easily detected by SXPS. The Mo 3d signal from a small amount of uncovered substrate would only cause a slight increase in the intensity on the high binding energy side of the Mo 3d spectrum. In the S 2p spectrum, the substrate peak strongly overlaps the Cr-S peak and, therefore, would be even more difficult to detect.

3.3 VALENCE-BAND SPECTROSCOPY

Valence-band spectra collected after Cr deposition and subsequent annealing are shown in Fig. 12. Valence-band spectra were collected with photon energies of 151 and 194 eV. Both sets of data were similar so only the 151 eV spectra are shown here. The valence-band spectrum taken from the clean $MoS_2(0001)$ surface is consistent with those published previously,[2,3,32] i.e., there is virtually identical orbital structure between 1.5 and 8.5 eV binding energy and the S 3s is at ~14 eV. (The two peaks at 9 and 11 eV are the result of excitation of S 2p photoelectrons by second-order light from the monochromator.)

There are several differences between the valence-band spectrum collected from the 5 Å Cr film and that of the clean surface. Although the MoS_2 peak structure is still present, there is a large increase in intensity between 0 and 3 eV due to the Cr 3d level. The appearance of a distinct Fermi edge and the increase in intensity from 0 to 1 eV show that the Cr film was essentially metallic. (Note that a small part of the metallic Fermi edge is due to metallic Mo at the film-substrate interface.) The intensity from the S 3s peak, as well as the peaks resulting from the S 2p core level in second order, decreased after depositing the 5 Å film since the substrate was covered by Cr. In addition, a 0.4 eV shift to lower binding energy, as a result of band bending, is seen for all valence-band features.

Changes similar to those seen in the 5 Å spectrum are observed in the spectra collected after deposition of 9 and 17 Å of Cr. Specifically, the MoS_2 valence-band features further decrease, the S 3s and 3p levels decrease, and the features corresponding to Cr increase. In fact, the valence-band spectra for 9 and 17 Å Cr are similar to spectra of pure Cr seen in a previous study.[33] The S 3p level is visible at ~5 eV, providing further evidence that some S was incorporated within the Cr overlayer.

When the 17 Å valence-band spectrum (which contains virtually no substrate signal) is appropriately scaled and subtracted from the 5 Å spectrum, the difference spectrum represents that portion of the valence band that does *not* have any contributions from the Cr-containing portion of the film. This difference spectrum, shown in Fig. 13, closely resembles the clean surface valence band with a small additional metallic contribution near the Fermi level. The metallic contribution is probably due to the metallic Mo reaction product that was present between the substrate and the Cr film since the larger contribution from the metallic Cr was subtracted out. The appearance of a difference spectrum with a structure so like that of the clean surface indicates that after Cr deposition the substrate is virtually the same, chemically and structurally, as the clean surface. Therefore, the interface between the reaction layer (i.e., the metallic Mo plus the partially reacted Cr film) and the $MoS_2(0001)$ substrate is abrupt. In other words, there is no intermixing of the Cr or the reaction products with the substrate. This indicates

that the reaction occurs at the substrate surface rather than by diffusion of Cr beneath the surface followed by MoS_2 decomposition.

Annealing the 17 Å film to progressively higher temperatures results in several changes in the valence-band spectra. The increases in the intensity between 3 and 7 eV (the S 3p region) and the sharpening of the Cr 3d peak at 1.5 eV after annealing to 425 °C indicate the formation of increased amounts of reacted Cr-S species. The narrow width of the Cr 3d peak suggests that it may represent a single Cr-S compound. In fact, the valence band of CrS is similar to that seen here.[27] Other Cr-S compounds, however, may have a similar valence-band structure, so it is difficult to identify a specific Cr-S phase based on the valence-band data. There is also a large decrease in the intensity between 0 and 1 eV after annealing to 425 °C, indicating that the Cr film surface is less metallic because of increased reaction with S. After annealing the film to 700 °C, and subsequently to 850 °C, the Fermi edge decreases further in size, confirming that little metallic Cr remains at the surface of the reaction layer. Some or all of the intensity at the Fermi edge may be due to the presence of the metallic Cr-Mo alloy near the film/substrate interface.

4. DISCUSSION

A better assessment of the reaction and growth mechanisms involved in the Cr/MoS_2(0001) system can be made by comparing the present results to those of previous high-resolution photoelectron spectroscopy studies of metal film growth on MoS_2(0001). Mn interacts strongly with the MoS_2(0001) surface forming MnS and metallic Mo.[3] Annealing the Mn-covered surface drives this reaction to completion. Fe, on the other hand, exhibits a relatively small reactivity with respect to MoS_2(0001).[2] The reaction of Fe with MoS_2(0001) results in the formation of an Fe-S surface phase and S-vacancy defects in the MoS_2 substrate rather than bulk iron sulfides and metallic Mo.[2] Annealing an Fe-covered surface causes the Fe film to agglomerate into Fe islands, primarily composed of metallic Fe, and uncovers the MoS_2(0001) surface. This indicates that the reaction of Fe with MoS_2(0001) to form bulk Fe sulfides is not favorable. In comparison with these two metals, Cr is more similar to Mn than to Fe, in that Cr also reacts with MoS_2(0001) during deposition, and the reaction is driven further on annealing. However, Mn is clearly more reactive than Cr since Mn reacts with MoS_2 to completion (all the Mn is converted to sulfidic form) on annealing to temperatures at which Cr only partially reacts.

The results of these three studies follow the trend predicted by bulk thermodynamics, although the reactions of other metals with MoS_2(0001) do not necessarily follow this trend.[1,5] For the reaction of Fe with MoS_2, a slightly positive Gibbs free energy of reaction ($\Delta G_{reaction}$ = +3.0 and +14.1 kcal/mole to form FeS and FeS_2, respectively)[1] indicates minimal reactivity. In contrast, Mn ($\Delta G_{reaction}$ = -25.2 kcal/mole to form MnS)[1] and Cr ($\Delta G_{reaction}$ = -10.1±4 kcal/mole to form CrS)[25,26] should both react with MoS_2, with Mn exhibiting the greater reactivity.

Fe, Cr, and Mn films form with varying morphologies on the MoS_2(0001) surface. Mn forms three-dimensional islands, and an equivalent thickness of 50 Å is required to cover the substrate with respect to the SXPS sampling depth. Fe and Cr, on the other hand, form relatively flat films that cover the substrate at equivalent thicknesses of 10 and 17 Å, respectively.

5. SUMMARY

The chemistry of the Cr/MoS_2(0001) interface was studied using SXPS and LEED. Vapor-deposited Cr formed a relatively flat overlayer composed primarily of metallic Cr. Cr partially reacted with the MoS_2(0001) surface to form metallic Mo and a Cr-S species. The Cr-S species was incorporated into the Cr overlayer with the S concentration enhanced at the surface of the film. Metallic Mo, on the other hand, formed near the film/substrate interface. In general, annealing a 17 Å film drove the reaction between Cr and the MoS_2 substrate. Annealing the Cr-covered sample to 425 °C resulted in slight agglomeration of the Cr overlayer and diffusion of additional S to the surface of the film to form an adsorbed S phase. Annealing to higher temperatures (700 °C and 850 °C) resulted in continued agglomeration of the Cr film, alloy formation between metallic Mo and Cr, and formation of two new adsorbed S species on the surface of the Cr-based film. The reactivity of Cr with MoS_2(0001) was shown to be greater than that of Fe and somewhat less than that of Mn.

The strong chemical interaction and lack of agglomeration at room temperature are indicators of good adhesion between metallic Cr and MoS_2. This fact could be exploited to provide improved adhesion between the solid lubricant MoS_2 and the surfaces of stainless (i.e., high-Cr) steel devices, providing an effective antiwear lifetime. However, an oxide layer is present or the steel surface, composed of Fe- and Cr-oxides, which precludes any but the weakest chemical interaction. Therefore, our results suggest that cleaning a steel surface to expose bare Fe and Cr metal before MoS_2 film deposition will increase the metal/lubricant adhesion.

REFERENCES

1. J.R. Lince, D.J. Carré, and P.D. Fleischauer, *Phys. Rev. B* **36** (1987) 1647.

2. J.R. Lince, T.B. Stewart, M.M. Hills, P.D. Fleischauer, J.A. Yarmoff, and A. Taleb-Ibrahimi, *Surf. Sci.* **223** (1989) 65.

3. J.R. Lince, T.B. Stewart, P.D. Fleischauer, J.A. Yarmoff, and A. Taleb-Ibrahimi, *J. Vacuum Sci. Technol.* A **7** (1989) 2469.

4. C.A. Papageorgopoulos and M. Kamaratos, *Surf. Sci.* **164** (1985) 353.

5. I.T. McGovern, E. Dietz, H.H. Rotermund, A.M. Bradshaw, W. Braun, W. Radlik, and J.F. McGilp, *Surf. Sci* **152/153** (1985) 1203.

6. M. Kamaratos and C.A. Pagageorgopoulos, *Surf. Sci.* **160** (1985) 451.

7. J.S. Zabinski and B.J. Tatarchuk, *Mater. Res. Soc. Symp. Proc.* **140** (1989) 239.

8. M. Kamaratos and C.A. Papageorgopoulos, *Appl. Surf. Sci.* **29** (1987) 279.

9. T.D. Durbin, J.R. Lince, and J.A. Yarmoff, *J. Vac. Sci. Technol. A* **10** (1992) 2529.

10. J. Bandet, A. Malvand, and Y. Quemener, *J. Phys. C* **13** (1980) 5657.

11. D.E. Eastman, J.J. Donelon, N.C. Hien, and F.J. Himpsel, *Nucl. Instrum. Methods* **172** (1980) 327.

12. F.J. Himpsel, Y. Jugnet, D.E. Eastman, J.J. Donelon, D. Grimm, G. Landgren, A. Marx, J.F. Morar, C. Oden, R.A. Pollak, J. Schneir, and C.A. Crider, *Nucl. Instrum. Methods* **222** (1984) 107.

13. S. Tanuma, C.J. Powell, and D.R. Penn, *Surf. Sci.* **192** (1987) L849.

14. D.A. Shirley, *Phys. Rev. B* **5** (1972) 4709.

15. J.R. Lince, T.B. Stewart, M.M. Hills, P.D. Fleischauer, J.A. Yarmoff, and A. Taleb-Ibrahimi, *Surf. Sci.* **210** (1989) 387.

16. J.C. Fuggle and N. Martensson, *J. Elect. Spectrosc. Relat. Phenom.* **21** (1980) 275.

17. S. Doniach and M. Sunjic, *J. Phys. C: Solid St. Phys.* **3** (1970) 285.

18. C.S. Fadley, in *Electron Spectroscopy: Theory, Techniques, and Applications*, edited by C. R. Brundle and A. D. Baker, (Academic Press, New York, 1978), Vol. 2, p. 70.

19. C.D. Wagner, W.M. Riggs, L.E. Davis, J.F. Moulder, and G.E. Muilenberg, *Handbook of X-ray Photoelectron Spectroscopy*, (Perkin-Elmer, Eden Prairie, MN, 1979).

20. J.J. Yeh and I. Lindau, *Atomic Data and Nuclear Data Tables* **32** (1985) 1.

21. K.S. Liang, S.P. Cramer, D.C. Johnston, C.H. Chang, A.J. Jacobson, J.P. deNeufville, and R.R. Chianelli, *J. Non-Cryst. Solids* **42** (1980) 345.

22. P.A.G. O'Hare, *J. Chem. Thermodynamics* **19** (1987) 675.

23. D.J. Young, W.W. Smeltzer, and J.S. Kirkaldy, *J. Electrochem. Soc.* **120** (1973) 1221.

24. K. Igaki, N. Ohashi, and M. Mikami, *J. Phys. Soc. Jpn.* **31** (1971) 1424.

25. K.C. Mills, *Thermodynamic Data for Inorganic Sulphides, Selenides, and Tellurides*, (Butterworths, London, 1974).

26. D.D. Wagman, W.H. Evans, V.A. Parker, R.H. Schumm, I. Halow, S.M. Bailey, K.L. Churney, and R.L. Nuttall, *NBS Tables of Chemical Thermodynamic Properties*, (AIP, New York, 1982); in: *J. Phys. Chem. Ref. Data 11, suppl. 2.*

27. J. Gopalakrishnan, T. Murugesan, M.S. Hedge, and C.N.R. Rao, *J. Phys. C: Solid State Phys.* **12** (1979) 5255.

28. D. Lichtman, J.H. Craig, V. Sailer, and M. Drinkwine, Appl. of *Surf. Sci.* **7** (1981) 325.

29. R.G. Musket, W. McLean, C.A. Colmenares, D.M. Makowiecki, and W.J. Siekhaus, *Appl. Surf. Sci* **10** (1982) 143.

30. A. Clark, N.B. Brookes, P.D. Johnson, M. Weinert, B. Sinkovic, and N.V. Smith, *Phys. Rev. B* **41** (1990) 9659.

31. M. Hansen and K. Anderko, *Constitution of Binary Alloys*, (McGraw-Hill Book Co. Inc., New York, 1958).

32. I. Abbati, L. Braicovich, C. Carbone, J. Nogami, I. Lindau, and U. del Pennino, *J. Electron Spectrosc. Related Phenomena* **40** (1986) 353.

33. H. Sugawara, K. Naito, T. Miya, A. Kakizaki, I. Nagakura, and T. Ishii, *J. Phys. Soc. Jap.* **53** (1984) 279.

Table 1. Measured binding energies of the Mo 3d and S 2p peaks (in eV) with respect to the Fermi level as a function of Cr deposition.[a]

Thickness	Binding Energy (eV)				
	S 2p			Mo 3d	
	S(substrate)	S(Cr-S)	$(S-S)^{2-}$	Mo(substrate)	Mo(metal)
Clean	162.4	---	---	229.5	---
0.3 Å	162.2	---	---	229.3	---
0.6 Å	162.2	---	---	229.2	---
2 Å	162.1	---	---	229.1	228.2
3 Å	162.1	162.0	---	229.1	228.2
4 Å	162.1	162.0	---	229.1	228.2
5 Å	162.1	162.0	163.5	229.1	228.2
7 Å	162.1	162.0	163.5	229.1	228.2
9 Å	---	162.0	163.5	229.0	228.1
12 Å	---	162.0	163.5	229.0	228.1
17 Å	---	162.1	163.5	229.0	228.1

[a] Binding energies are taken from least-squares fits of the low kinetic energy photoelectron spectra (i.e., hν=300 and 230 eV for Mo 3d and S 2p, respectively). High kinetic energy binding energies vary by ≤0.1 eV from these values.

Table 2. Measured binding energies of the Mo 3d and S 2p peaks (in eV) with respect to the Fermi level as a function of annealing temperature for a 17 Å Cr film.[a]

Anneal Temp.	Binding Energy (eV)				
	S 2p				Mo 3d
	S(Cr-S)	S(adsorbed,1)	S(adsorbed,2)	$(S-S)^{2-}$	Mo(metal) [Mo(alloy)]
No anneal	162.1	---	---	163.5	228.1
425 °C	161.9	161.1	---	163.5	227.9
700 °C	162.0	161.4	160.7	163.5	[228.3]
850 °C	162.1	161.4	160.8	163.5	[228.4]

[a] Binding energies are taken from least-squares fits of the low kinetic energy photoelectron spectra (i.e., hν=300 and 230 eV for Mo 3d and S 2p, respectively). High kinetic energy binding energies vary by ≤0.1 eV from these values.

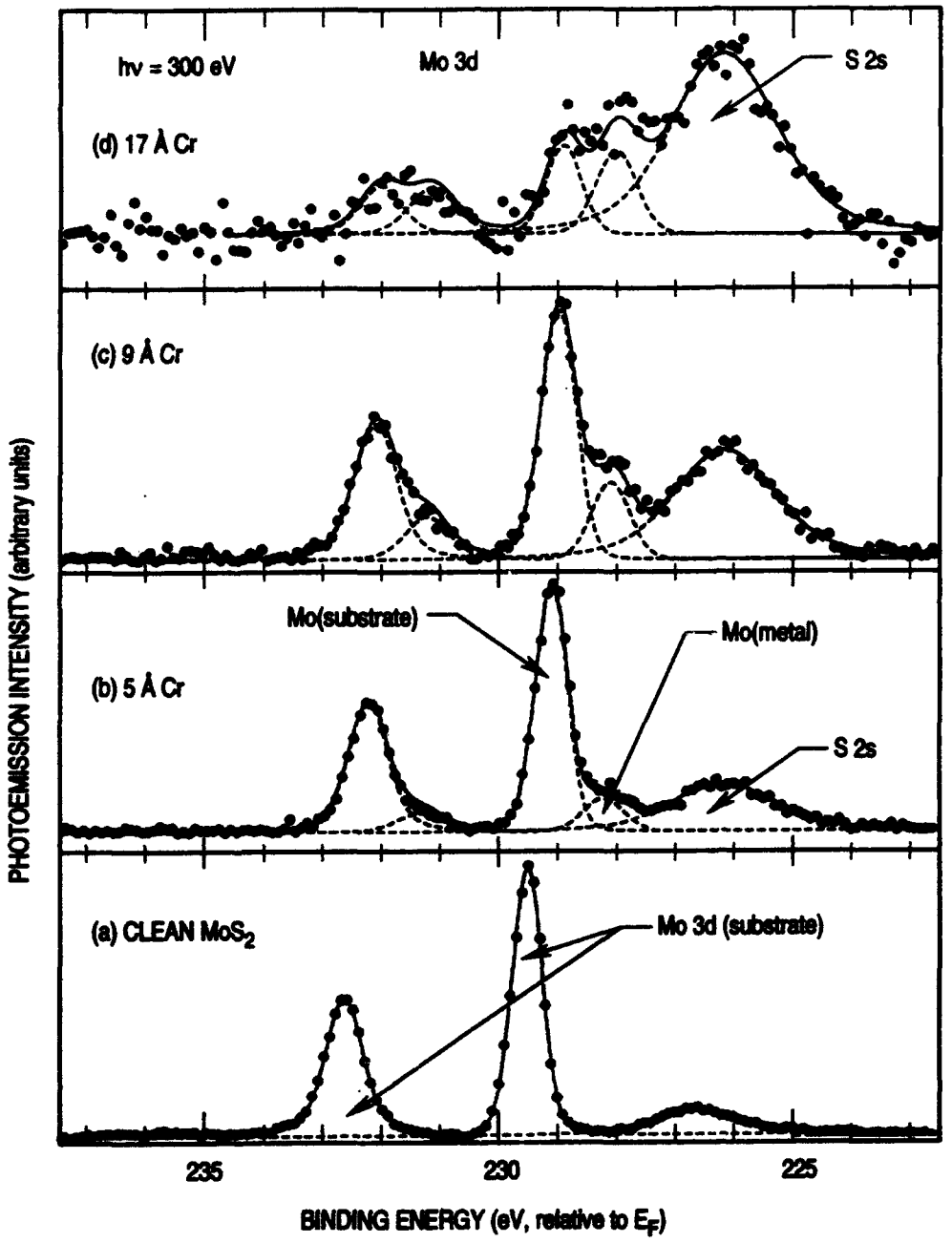

Figure 1. Representative Mo 3d core-level spectra taken after various depositions of Cr onto the $MoS_2(0001)$ surface. The spectra were collected at a photon energy of 300 eV, producing photoelectrons with a kinetic energy of ~70 eV. Spectra corresponding to the clean surface and depositions of 5, 9, and 17 Å of Cr are shown. The dots are the raw data points after background subtraction, the dashed lines are the individual components of the numerical fit, and the solid line is the resultant fit. Binding energies are relative to the Fermi energy, and the spectra are all scaled to approximately equal peak heights.

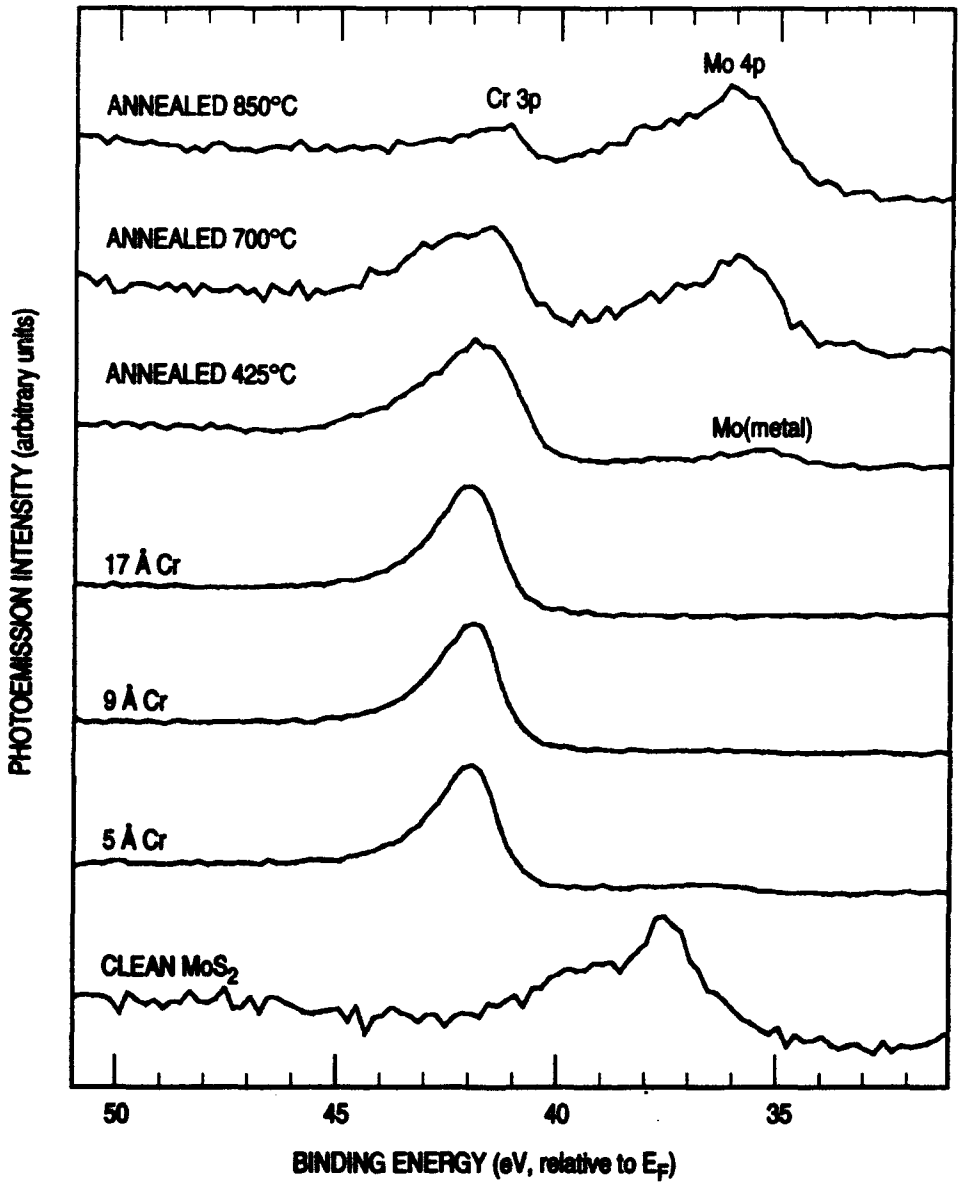

Figure 2. Representative Cr 3p and Mo 4p core-level spectra collected after several depositions of Cr and after annealing the Cr-covered surface. The spectra were collected with a photon energy of 151 eV. The spectra collected from the clean surface, and after Cr films of 5, 9, and 17 Å thickness are shown, as well as the 17 Å film after annealing to 425 °C, 700 °C, and 850 °C. The spectra are all scaled to approximately equal peak heights.

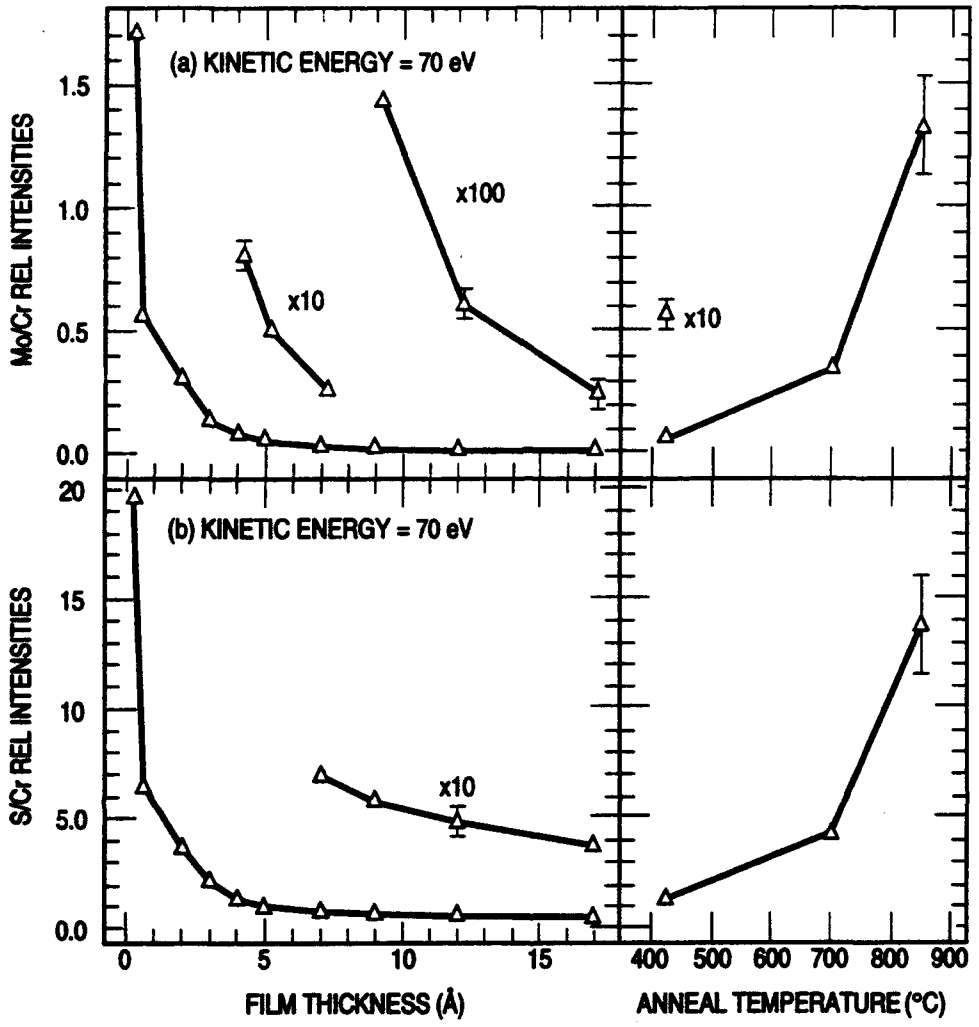

Figure 3. Ratios of (a) the total Mo 3d peak area to the total Cr 3p peak area and (b) the total S 2p peak area to the total Cr 3p peak area, both plotted versus film thickness. The peak areas were corrected for differences in photon-energy-dependent cross section and photoelectron escape depth, so these curves correspond approximately to relative atomic amounts within the SXPS detection depth. The ratios were determined from Mo 3d, S 2p and Cr 3p spectra collected for photon energies of 300, 230, and 151 eV, corresponding to photoelectron kinetic energies of ~70, ~70, and ~100 eV, respectively. These kinetic energies correspond to average photoelectron escape depths of 3.0 Å for both S 2p and Mo 3d, and 3.5 Å for Cr 3p. The lines are drawn as an aid to the reader and are not intended to suggest linear trends between the data points. Representative error bars are shown on the graph.

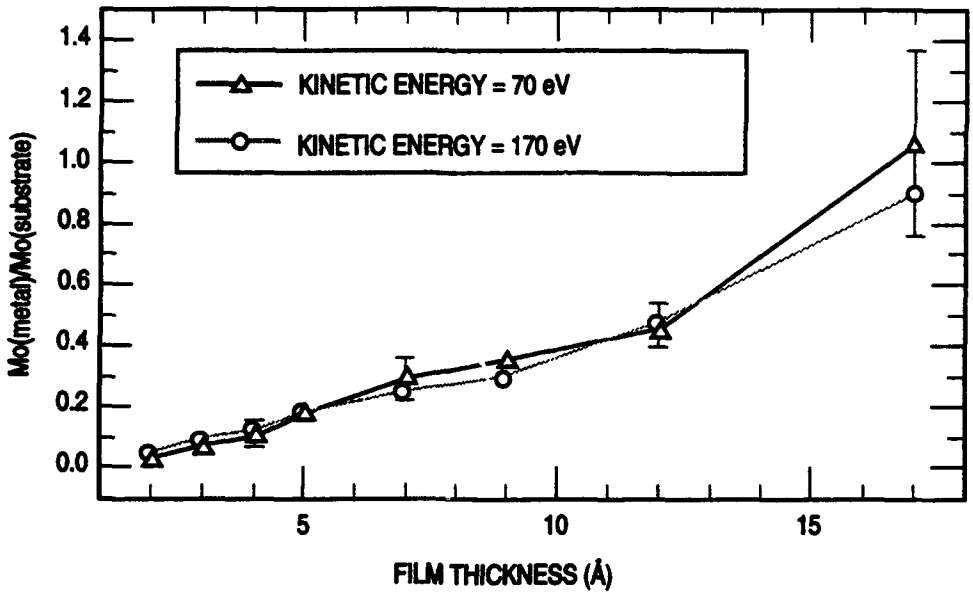

Figure 4. The ratio of the metallic Mo 3d peak area to the substrate Mo 3d peak area versus film thickness. The ratios were calculated from spectra collected with photon energies of 300 and 400 eV, resulting in photoelectron kinetic energies of ~70 and ~170 eV, respectively. These kinetic energies correspond to average photoelectron escape depths of 3.0 Å and 4.7 Å, respectively. The lines are drawn as an aid to the reader and are not intended to suggest linear trends between the data points. Representative error bars are shown on the graph.

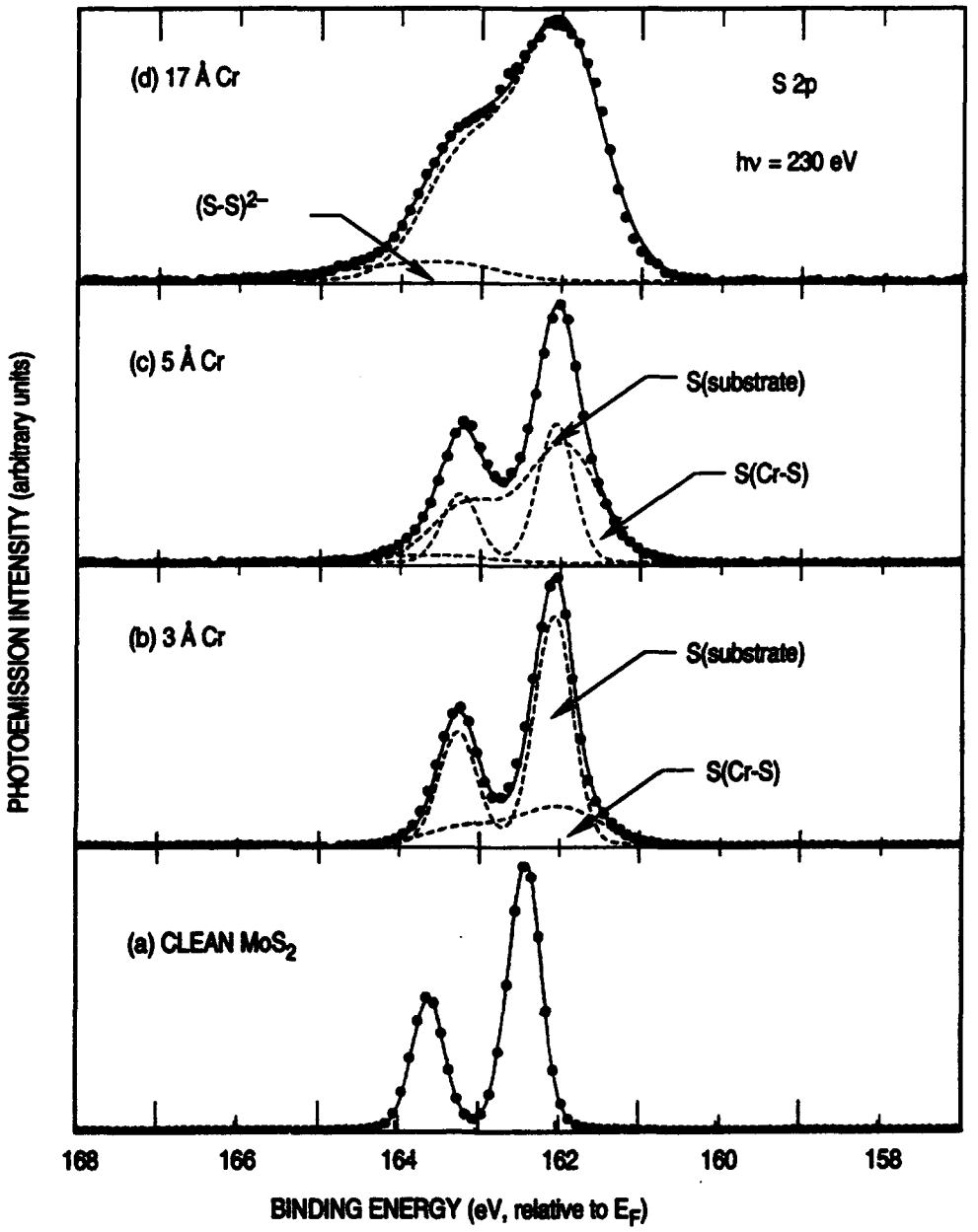

Figure 5. Representative S 2p core-level spectra taken after several depositions of Cr onto the $MoS_2(0001)$ surface. The spectra were taken at a photon energy of 230 eV, which corresponds to a photoelectron kinetic energy of ~70 eV. Spectra collected from the clean surface and after depositions of 3, 5, and 17 Å are shown. The dots are the raw data points after background subtraction, the dashed lines are the individual components of the numerical fit, and the solid line is the sum of these components. The spectra are all scaled to approximately equal peak heights.

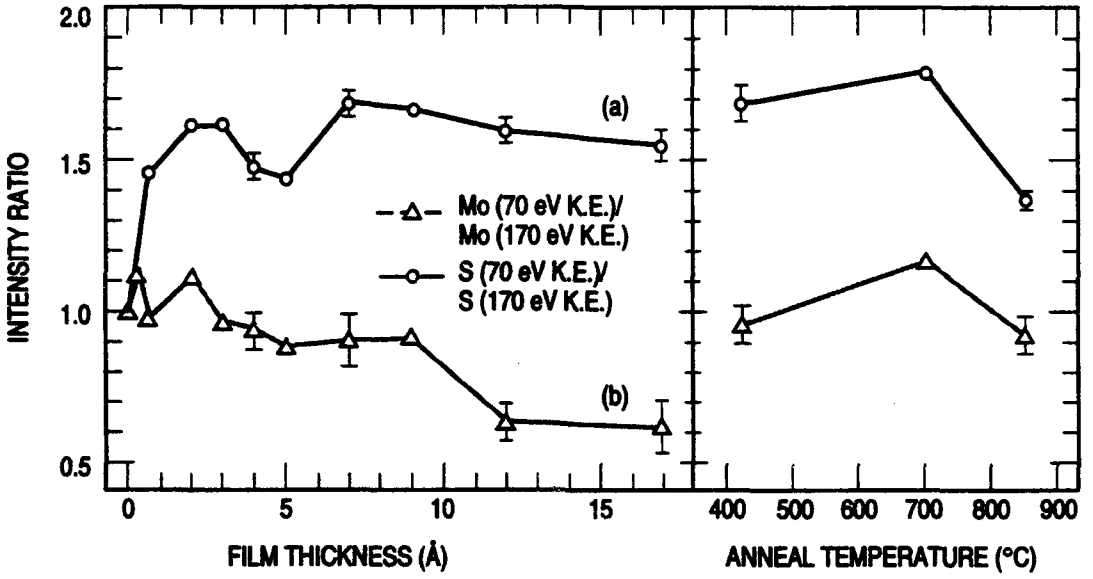

Figure 6. Ratios of (a) the total S 2p peak area for low photoelectron kinetic energy (~70) to that for high photoelectron kinetic energy (~170) and (b) the total Mo 3d peak area for low photoelectron kinetic energy (~70) to that for high photoelectron kinetic energy (~170), both plotted versus film thickness. Photoelectron kinetic energies of ~70 and ~170 eV correspond to average photoelectron escape depths of 3.0 Å and 4.7 Å, respectively. The curves were normalized so that the ratios at zero coverage were equal to 1.0 for both S and Mo. Therefore, values >1.0 represent S or Mo that is enhanced at the surface with respect to S or Mo present at the clean MoS_2(0001) surface. The lines are drawn as an aid to the reader and are not intended to suggest linear trends between the data points. Representative error bars are shown on the graph.

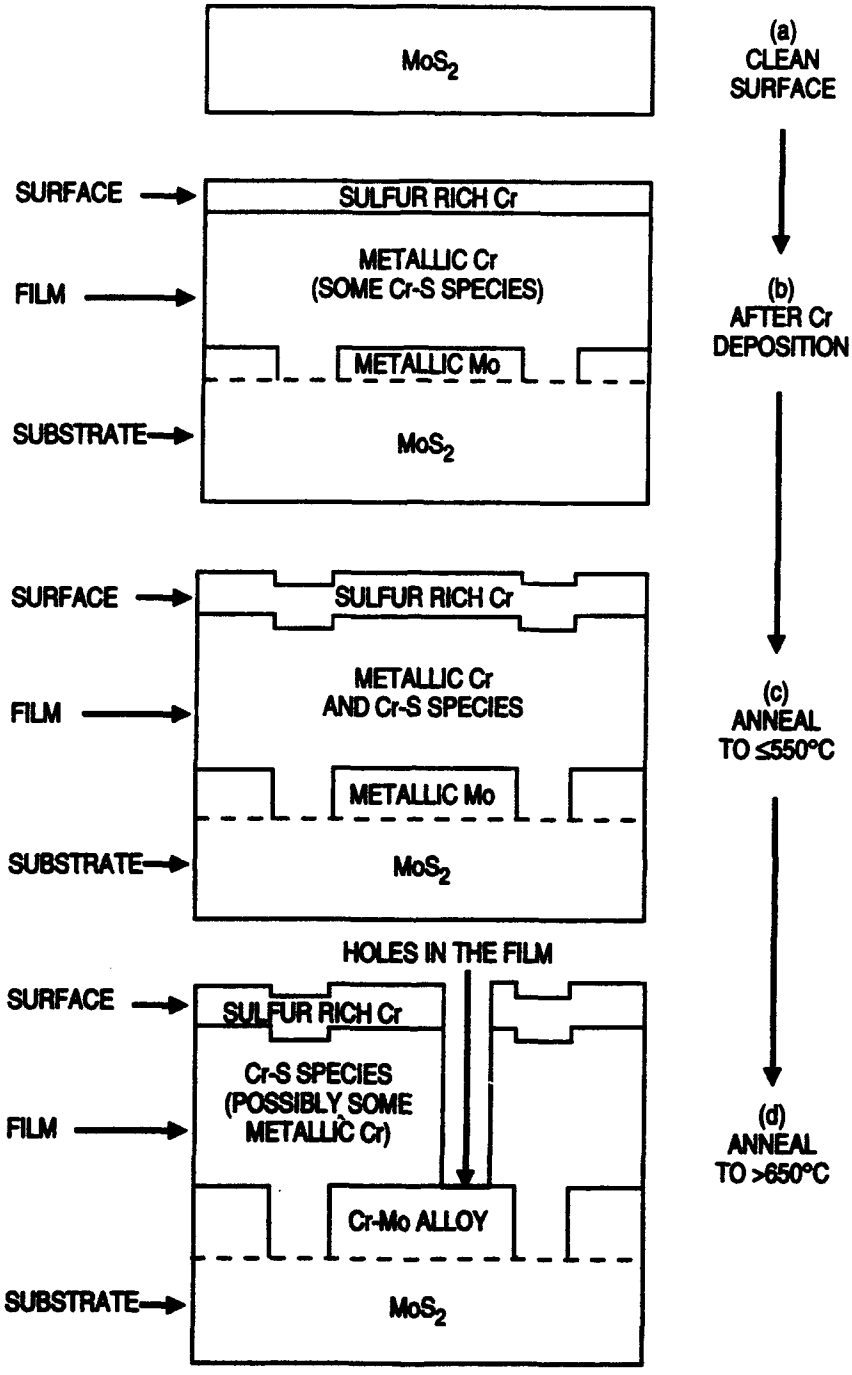

Figure 7. A schematic representation of the reaction layer after deposition and annealing of a 17 Å Cr film on MoS_2(0001). This figure is based on the results of the present study as well as those of Ref. 9. Moving downward on the figure [i.e., from (b) to (c) to (d)] corresponds with increasing amounts of metallic Mo and reacted Cr-S species, with a concurrent decrease in the amount of metallic Cr.

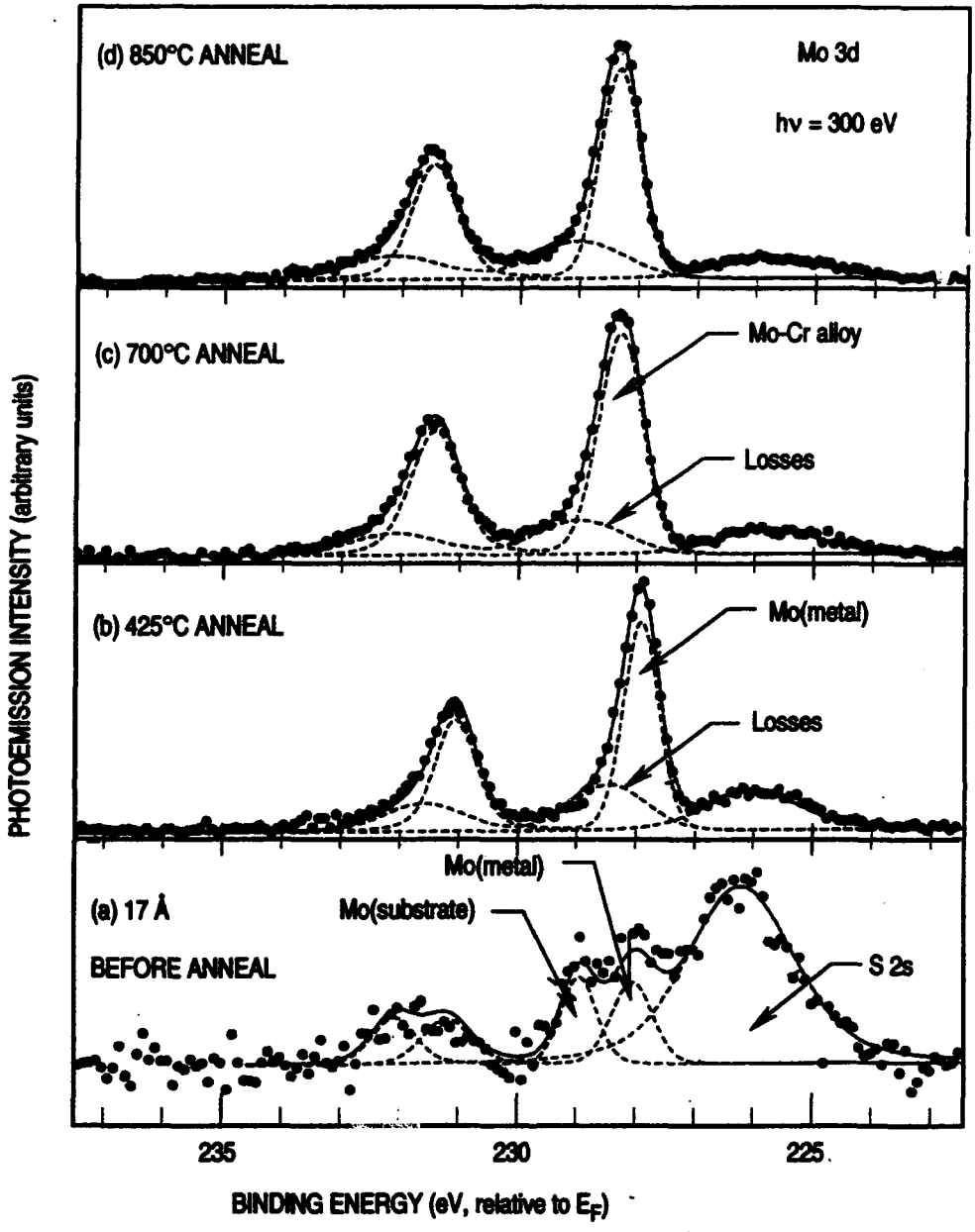

Figure 8. Mo 3d core-level spectra collected after annealing the Cr-covered $MoS_2(0001)$ surface. The spectra were taken at a photon energy of 300 eV, corresponding to a photoelectron kinetic energy of ~70 eV. The spectra for the 17 Å Cr film as well as those collected from the 17 Å film annealed to 425 °C, 700 °C, and 850 °C are shown. The spectra are all scaled to approximately equal peak heights.

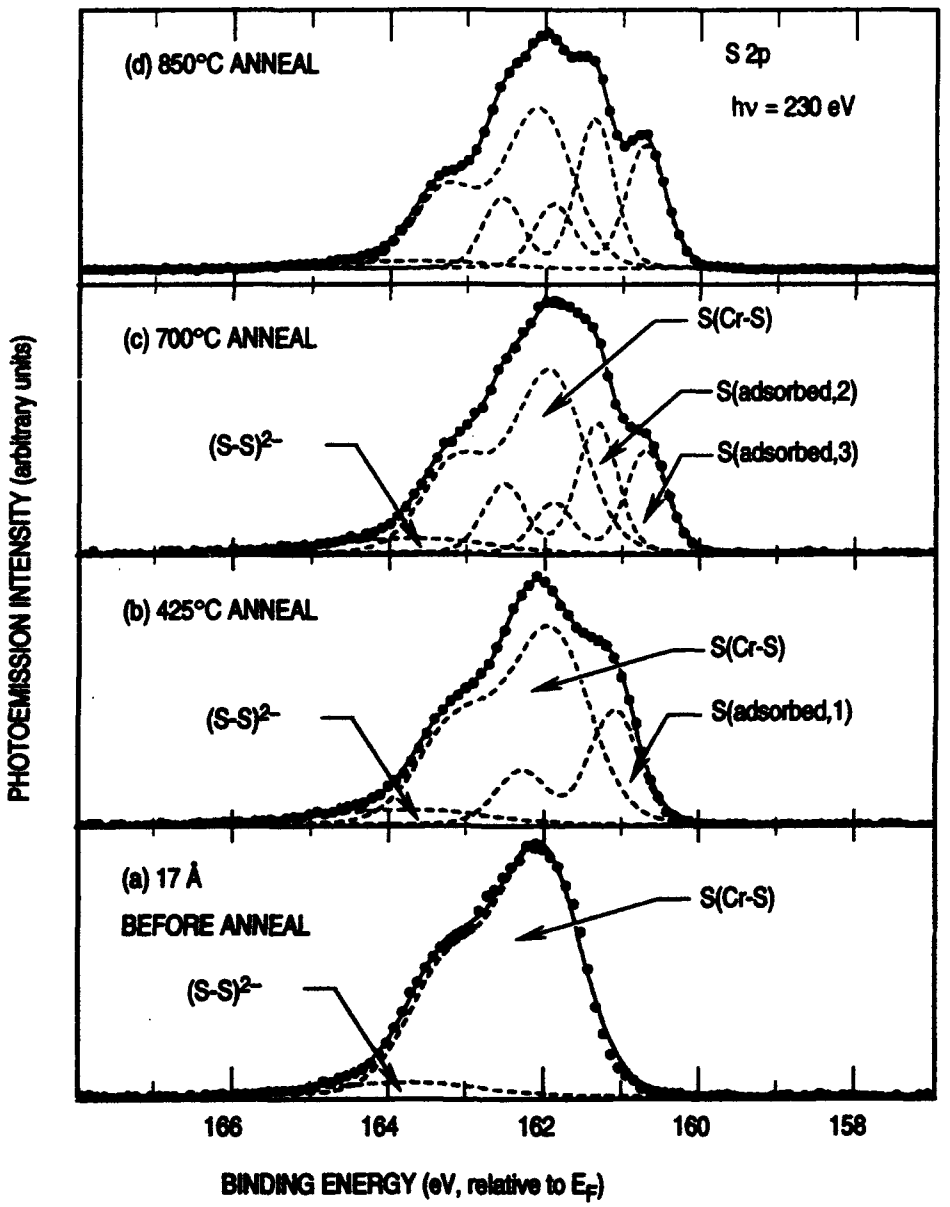

Figure 9. S 2p core-level spectra collected after annealing the Cr-covered $MoS_2(0001)$ surface. The spectra were taken at a photon energy of 230 eV, which corresponds to a photoelectron energy of 70 eV. The spectra for the 17 Å film as well as those collected from the 17 Å film annealed to 425 °C, 700 °C, and 850 °C are shown. The spectra are all scaled to approximately equal peak heights.

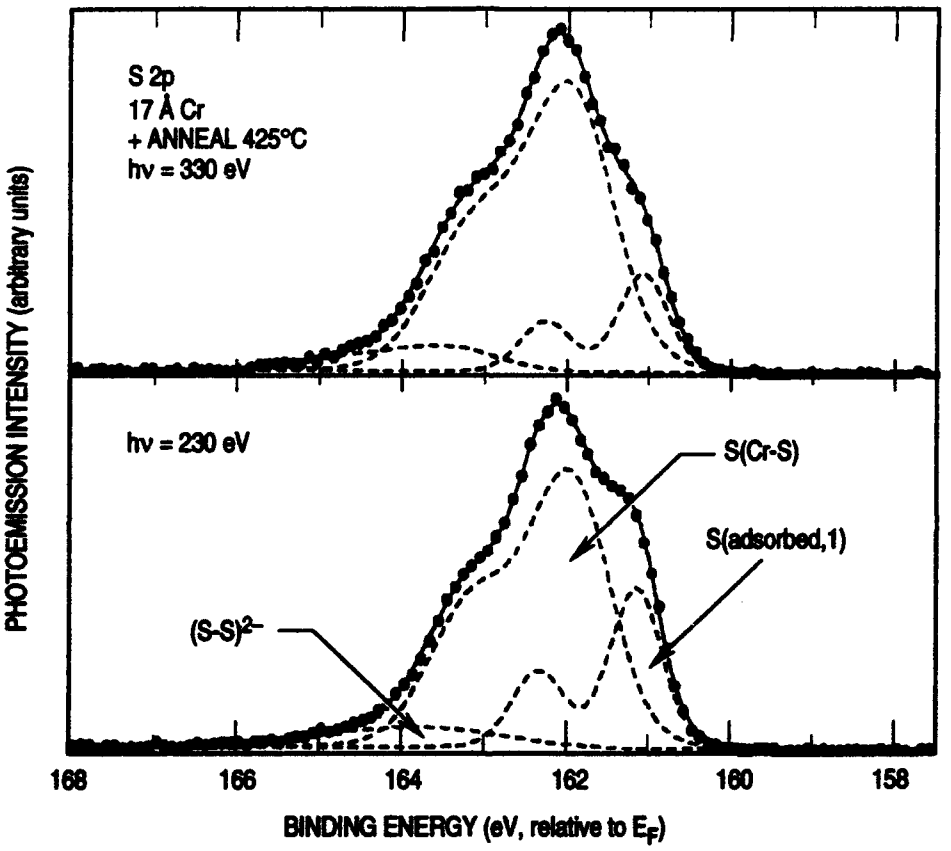

Figure 10. S 2p core-level spectra collected after annealing the Cr-covered MoS_2(0001) surface to 425 °C. The spectra were collected employing photon energies of 230 and 330 eV, resulting in photoelectron kinetic energies of ~70 and ~170 eV, respectively.

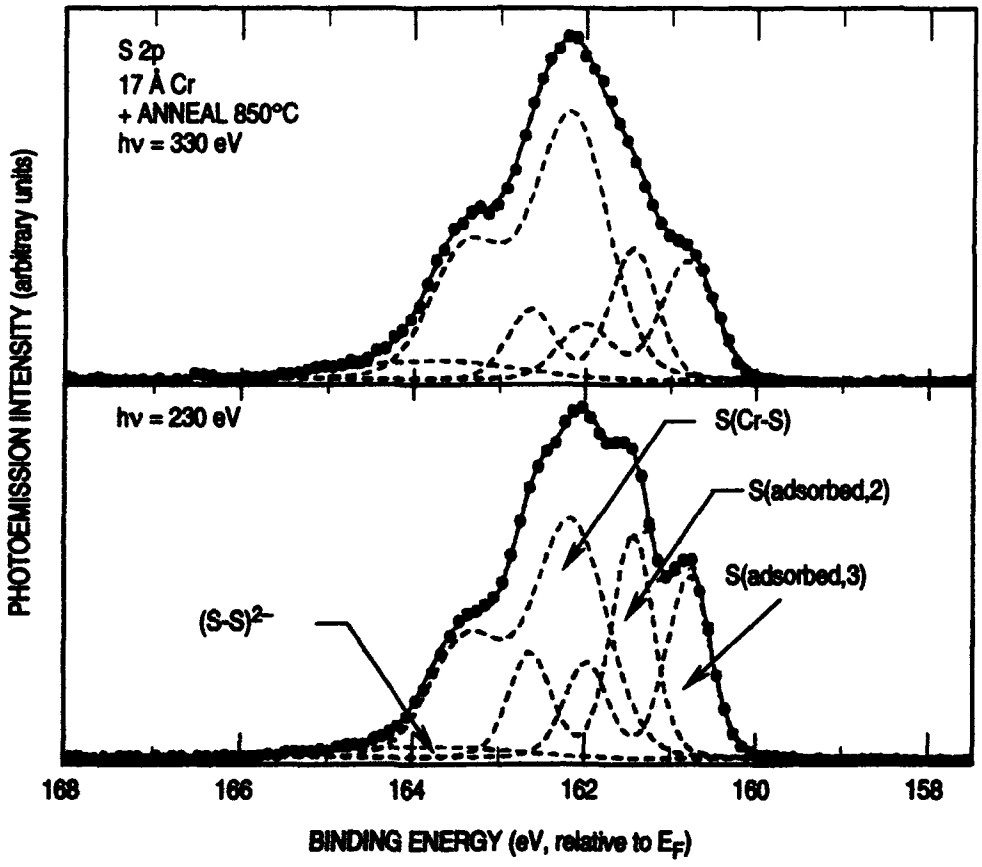

Figure 11. S 2p core-level spectra collected after annealing the Cr-covered $MoS_2(0001)$ surface to 850 °C. The spectra shown were collected employing photon energies of 230 and 330 eV, resulting in photoelectron kinetic energies of ~70 and ~170 eV, respectively.

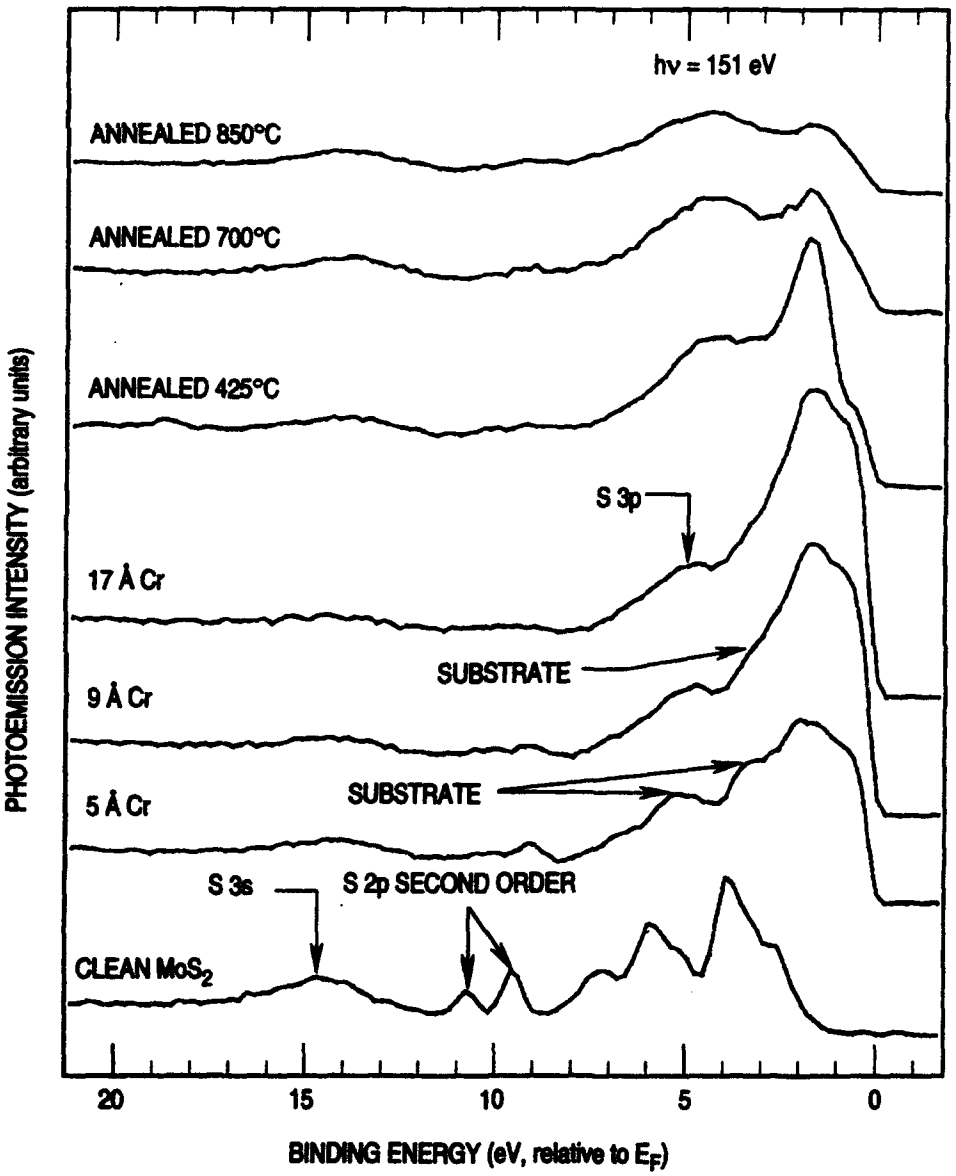

Figure 12. Valence-band spectra collected after depositing Cr on the MoS_2(0001) surface. The spectra were taken at a photon energy of 151 eV. The spectra collected of the clean surface and after Cr films of 5, 9, and 17 Å were deposited. Also shown are spectra for the 17 Å Cr film annealed to 425 °C, 700 °C, and 850 °C.

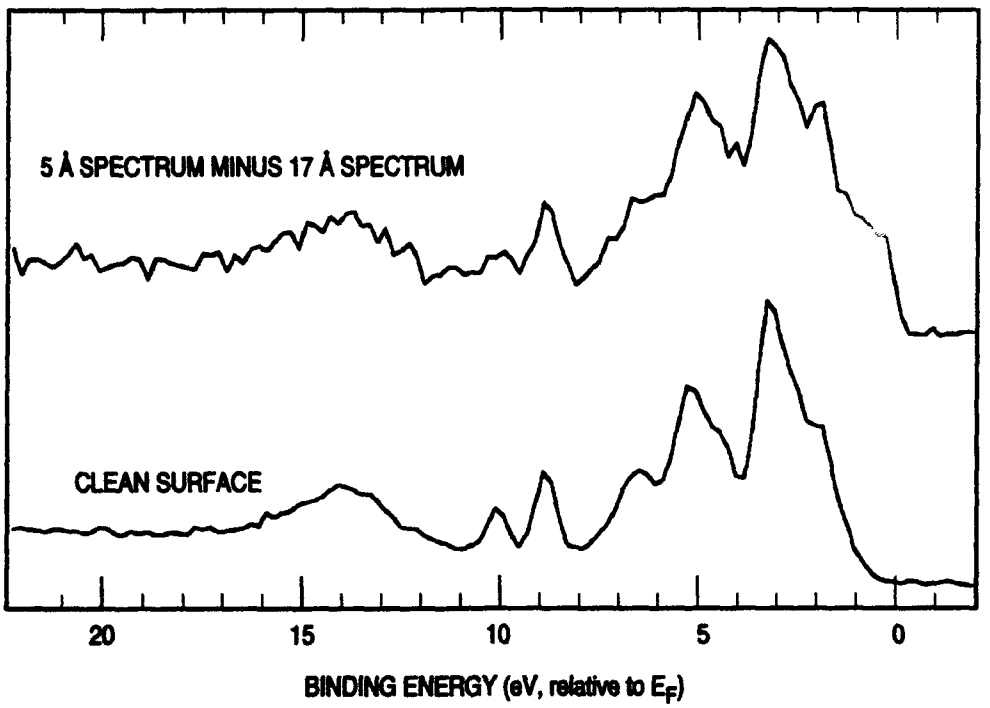

Figure 13. Valence-band difference spectrum obtained by scaling and subtracting the valence-band spectrum for the 17 Å film from that of the 5 Å film. The clean surface is shown for comparison. The clean surface valence-band spectrum shown was shifted 0.4 eV to compensate for band bending.

TECHNOLOGY OPERATIONS

The Aerospace Corporation functions as an "architect-engineer" for national security programs, specializing in advanced military space systems. The Corporation's Technology Operations supports the effective and timely development and operation of national security systems through scientific research and the application of advanced technology. Vital to the success of the Corporation is the technical staff's wide-ranging expertise and its ability to stay abreast of new technological developments and program support issues associated with rapidly evolving space systems. Contributing capabilities are provided by these individual Technology Centers:

Electronics Technology Center: Microelectronics, solid-state device physics, VLSI reliability, compound semiconductors, radiation hardening, data storage technologies, infrared detector devices and testing; electro-optics, quantum electronics, solid-state lasers, optical propagation and communications; cw and pulsed chemical laser development, optical resonators, beam control, atmospheric propagation, and laser effects and countermeasures; atomic frequency standards, applied laser spectroscopy, laser chemistry, laser optoelectronics, phase conjugation and coherent imaging, solar cell physics, battery electrochemistry, battery testing and evaluation.

Mechanics and Materials Technology Center: Evaluation and characterization of new materials: metals, alloys, ceramics, polymers and their composites, and new forms of carbon; development and analysis of thin films and deposition techniques; nondestructive evaluation, component failure analysis and reliability; fracture mechanics and stress corrosion; development and evaluation of hardened components; analysis and evaluation of materials at cryogenic and elevated temperatures; launch vehicle and reentry fluid mechanics, heat transfer and flight dynamics; chemical and electric propulsion; spacecraft structural mechanics, spacecraft survivability and vulnerability assessment; contamination, thermal and structural control; high temperature thermomechanics, gas kinetics and radiation; lubrication and surface phenomena.

Space and Environment Technology Center: Magnetospheric, auroral and cosmic ray physics, wave-particle interactions, magnetospheric plasma waves; atmospheric and ionospheric physics, density and composition of the upper atmosphere, remote sensing using atmospheric radiation; solar physics, infrared astronomy, infrared signature analysis; effects of solar activity, magnetic storms and nuclear explosions on the earth's atmosphere, ionosphere and magnetosphere; effects of electromagnetic and particulate radiations on space systems; space instrumentation; propellant chemistry, chemical dynamics, environmental chemistry, trace detection; atmospheric chemical reactions, atmospheric optics, light scattering, state-specific chemical reactions and radiative signatures of missile plumes, and sensor out-of-field-of-view rejection.